BatDeck: Advancing Nano-drone Navigation with Low-power Ultrasound-based Obstacle Avoidance

Hanna Müller*, Victor Kartsch*, Michele Magno*, Luca Benini*†

*Integrated Systems Laboratory / Center for Project-Based Learning - ETH Zürich, Switzerland

†DEI - University of Bologna, Italy

Email: {hannuell, vkartsch, mmagno, lbenini}@ethz.ch

Abstract—Nano-drones, distinguished by their agility, minimal weight, and cost-effectiveness, are particularly well-suited for exploration in confined, cluttered and narrow spaces. Recognizing transparent, highly reflective or absorbing materials, such as glass and metallic surfaces is challenging, as classical sensors such as cameras or laser rangers often do not detect them. Inspired by bats, which can fly at high speeds in complete darkness with the help of ultrasound, this paper introduces BatDeck, a pioneering sensor-deck employing a lightweight and low-power ultrasonic sensor for nano-drone autonomous navigation. This paper first provides insights about sensor characteristics, highlighting the influence of motor noise on the ultrasound readings, then it introduces the results of extensive experimental tests for obstacle avoidance (OA) in a diverse environment. Results show that BatDeck allows exploration for a flight time of 8 minutes while covering 136m on average before crash in a challenging environment with transparent and reflective obstacles, proving the effectiveness of ultrasonic sensors for OA on nano-drones.

Index Terms—nano-drone, nano-UAV, ultrasound, obstacle avoidance, autonomous navigation

I. INTRODUCTION

The global drone market, with a projected value of \$54.6 billion by 2030 [1], reflects this technology's rapid growth and increasing relevance due to its versatility for various applications, ranging from agriculture, construction, and public safety to urban planning. While larger drones are known for their capability to execute complex tasks, nano-drones offer unique advantages, especially in constrained environments like greenhouses and buildings. Their small size (typically $\sim 10~\rm cm$ diameter [2]) makes them safer for people and property. Given its versatility and modularity, the Crazyflie 2.1 (CF), an open software, open hardware nano-drone, has gained popularity among research and commercial entities [3]–[7].

A critical aspect of ensuring the drone platform's safe and efficient operation is obstacle avoidance (OA). OA requires appropriate sensing technologies that typically include light detection and ranging (LiDAR), Radio Detection and Ranging (RADAR), cameras [3], [4], [7], and laser-based time-of-flight (ToF) sensors [5], [7]. However, LiDAR and RADAR are bulky and power-hungry, which forbid their use for nanodrones applications, while cameras and laser-based ToF sensors do not perform well when dealing with reflective surfaces or transparent barriers such as glass walls. Although sensor fusion of multiple powerful onboard sensors allows larger

Identify applicable funding agency here. If none, delete this.

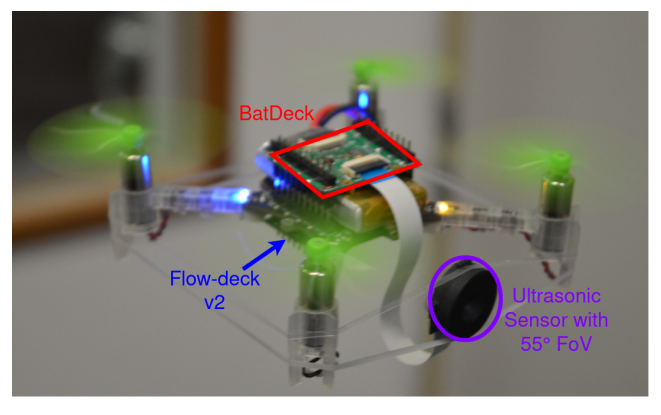


Fig. 1: The Crazyflie 2.1 with the *BatDeck* and the Flow-deck v2, during an OA test flight.

drones to overcome inaccurate measurements, nano-drones, typically below 50 g, must resort to lightweight and low-power sensors due to their payload and power limitations [2]. Taking inspiration from the echolocation techniques employed by bats and dolphins, ultrasound (US) sensors, which measure the ToF in echos of high-frequency sound, are a promising alternative, offering better performance when dealing with sound-reflecting objects independently of color, transparency, or texture [8], [9].

A wide range of ultrasonic sensors applicable for use in robotics are currently available on the market and have been examined in the literature [10], [11]. However, their size, weight, and energy requirements preclude their use in nano-drone applications. The recently introduced ICU-30201 sensor from TDK overcomes these limitations with its ultralow power consumption (below $1\,\mathrm{mW}$) and compact form factor $(5.17\times2.68\times0.9\,\mathrm{mm})$, making it an ideal choice for integration into small-scale robotic platforms [12]. Exploiting this novel US sensor, we move nano-drones toward bat-like navigation with our four main contributions:

(1) Design and implementation of an US extension for nanodrones: This contribution focuses on the design and characterization of an US-based perception system for nano-drones (shown in Figure 1). We integrate the compact and energyefficient ICU-30201 sensor into the drone's architecture, enabling it to emit and receive ultrasonic signals for obstacle detection and navigation, akin to the natural echolocation used by bats.

- (2) Characterization and countermeasures against motor noise: Vibrations affect US sensors. Therefore, we characterize the noise and evaluate filtering methods to extract the echolocation signal. We also characterize the US obstacle detection performance at different distances and angles towards concrete and glass surfaces.
- (3) Implementation and evaluation of an OA algorithm tailored for resource-constrained hardware (ARM Cortex-M4) onboard a nano-drone in terms of power, latency, and memory requirements.
- (4) In-field evaluation and comparison with laser-based ToF sensors in OA applications: The final section presents an infield evaluation of the nano-drone equipped with the *BatDeck*, comparing its OA capabilities against a more conventional laser-based ToF system. This analysis focuses on effectiveness, power consumption, and adaptability to various environments, providing insights into the advantages and potential limitations of US versus laser-based ToF sensors in real-world applications and OA scenarios.

II. RELATED WORK

OA can rely on several sensing sources, including Li-DAR, RADAR, cameras, laser-based ToF, and US sensors. LiDAR sensors reconstruct a 3D space using consecutive range measurements projected in all directions sequentially. While LiDAR technology is one of the best solutions for OA, its power consumption and size are incompatible with nanodrones.

Cameras have also been used successfully for OA tasks. Tiny, low-power cameras can easily be mounted and operated on small systems such as nano-drones. For instance, authors in [13] designed a vision-based CF-compatible shield for OA. The device integrates a low-power monochrome QVGA camera (Himax HM01B0) and GAP8, an Parallel Ultra-Low-Power (PULP) system-on-chip (SoC) for efficient computation. The navigational commands are based on PULP-DroNet, a convolutional neural network for OA fine-tuned for this platform. Authors in [3] use a lightweight CNN depth estimation network for OA - the generated depth map could even be used for path planning. While camera-based approaches are compatible with nano-drones, they still lack performance in poor lighting conditions or when navigating across an environment with objects that have not been included in the training sets.

Authors in [7] have recently presented Stargate, a multimodal sensor fusion system for nano-drones, enabling autonomous navigation and gate detection through sensor fusion between a low-power grayscale camera (Himax HM01B0) and a multi-pixel (8x8) laser-based ToF (VL53L5CX) sensor from STMicroelectronics. The system is trained entirely on synthetic data and tested on a CF drone, demonstrating robust navigation with a low failure rate in various scenarios. While this approach is working in many environments, its robustness can be improved with fusing an additional sensor perceiving glass or visually reflective materials correctly.

Attempting to take advantage of sound, which can also detect visually transparent and shiny obstacles, Duembgen et al. [14] developed a real-time, model-based system for auditory localization and mapping tailored for compact robots. Using buzzers and basic microphones, the system achieves centimeter precision without prior calibration or training. However, applying this method onboard nano-drones presents challenges due to the constraints related to weight and size, as well as interference with audible motor noise, rendering it impractical for such applications.

Recent advancements in micro-electromechanical systems (MEMS) design have enabled the development of new technologies that are low-power, lightweight, and compact. The ICU-30201 ultrasonic ToF incorporates Aluminum Nitride (AlN) piezoelectric micromachined ultrasonic transducers (PMUTs) to offer enhanced sensitivity and reduced power consumption when compared to traditional piezoceramic transducers. Furthermore, its size and weight are compatible with nano-drones.

In this paper, we leverage the capabilities of the TDK ICU-30201 to develop *BatDeck*, an expansion board compatible with CF drones, enhancing their performance for OA tasks. We detail the sensor's characterization under various flight conditions and across different materials and provide a quantitative assessment of its efficacy in complex environments compared to conventional laser-based ToF sensors.

III. HARDWARE SETUP

In this section, we introduce the ICU-30201, the US sensor used in this paper, as well as details on the *BatDeck*, our custom-designed expansion deck. In the following, we also introduce details about our flying platform, the CF drone.

A. ICU-30201

The ICU-30201 is a miniature, ultra-low power MEMS-based ultrasonic ToF transceiver. It integrates a nominally $f_{op} = 50kHz$ PMUT and a 40 MHz CPU for sampling and pre-processing. It can record maximally 340 in-phase and quadrature (IQ) data samples per measurement, converted to baseband. The output data rate (ODR) can be configured as $ODR = f_{op}/N$ where N = 2, 4, 8. The IQ allows computing phase and magnitude of the reflected US waves.

B. BatDeck

This section presents the design and implementation of the *BatDeck*, a custom-made extension deck for the Crazyflie, which features four slots for attaching TDK ICU-x0201 sensors. In this work, we only use one slot to attach a forward-facing ICU-30201 ultrasonic sensor with a 55° field-of-view (FoV) horn, attached to the drone with two rubber bands (for dampening). The *BatDeck* with one sensor weighs in total 3 g, where the expansion deck PCB itself contributes 1.37 g, the sensor horn 1.25 g.

C. Crazyflie Platform

This work employs the CF from Bitcraze, a 10-centimeter nano-drone featuring an STM32F405 microcontroller unit (MCU), which oversees state estimation and actuation control. The drone is also equipped with a Flow-deck v2, which enables optical flow and height measurements to improve state estimation. We use $7\times16~\mathrm{mm}$ 19000 KV motors from betafpv, 47-17 propeller from Bitcraze, and an $350~\mathrm{mAh}$ LiPo battery from Tattu. This base configuration weighs $34~\mathrm{g}$.

IV. SENSOR AND NOISE CHARACTERIZATION AND CALIBRATION

This section presents a performance evaluation of the ultrasonic sensor in the presence of motor noise (during flight), maximum range, and measurement performance for angled obstacles. Transmission/Reception commands can be configured in cycles of the MUTCLK, which operates at $16 \times f_{op}$. We configure the sensor to transmit for 512 cycles and actively dampen ringdown artifacts for an additional 45 cycles. We chose N=4, giving us a range of $4.6\,\mathrm{m}$ and a resolution of $1.35\,\mathrm{cm}$ (with $f_{op}=50kHz$ and 340 samples per measurement). Note that f_{op} can change from sensor to sensor and in different environmental conditions.

Measurement acquisition runs at $33\,\mathrm{Hz}$, however, the radio-based transmission is limiting the logging frequency. Considering that the phase information is not used in this paper, we directly stream out magnitude data (instead of transmitting IQ parameters), at a measurement rate of $\sim\!4.8\,\mathrm{Hz}$. The magnitude data corresponds to the intensity of the received US wave, which we can use to detect sound-reflecting objects and calculate the distances to them. As the drone's motor vibrations lead to noise on the sensor data, we first characterize the noise induced by the motors and later evaluate the sensor performance.

A. Motor Noise

To characterize the motor noise, we configure the ICU-30201 to only receive (i.e., no US waves are emitted) while the drone hovers at $0.7\,\mathrm{m}$.

The goal is to increase signal-to-noise ratio (SNR) by filtering out the motor noise to be able to detect the reflected signal from the closest obstacle, while choosing an algorithm with low computational and memory requirements for onboard execution. Filtering can be applied on both slow-time (i.e., over consecutive US measurements) or fast-time (i.e., over the consecutive 340 US samples from the same measurement).

To save memory, we use an exponentially moving average in slow-time: $y_{i_n} = \frac{K_s-1}{K_s}y_{i_{n-1}} + \frac{1}{K_s}x_{i_n}$ where n denotes the measurement number and i the sample number within the measurement, y denotes the filtered magnitude while x is the raw measurement. In fast-time, we use a averaging filter: $y_{i_n} = \sum_{j=i-K_f+1}^{i} \frac{x_{j_n}}{K_f}$. In Figure 2, we show the standard deviation, median, and

In Figure 2, we show the standard deviation, median, and outliers of the motor induced noise on the sensor signal. We evaluate the unfiltered baseline $(K_s = 1, K_f = 1)$ against $K_f = 3$, $K_s = 3$ and $K_s = 5$. As shown in Figure 2, filtering

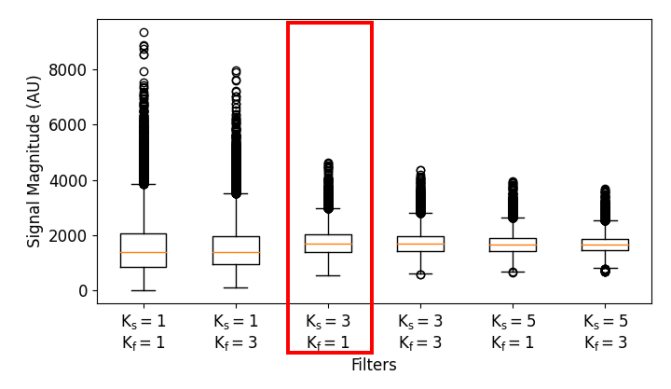


Fig. 2: The effect of different filter lengths in slow and fast time to the motor noise standard deviation.

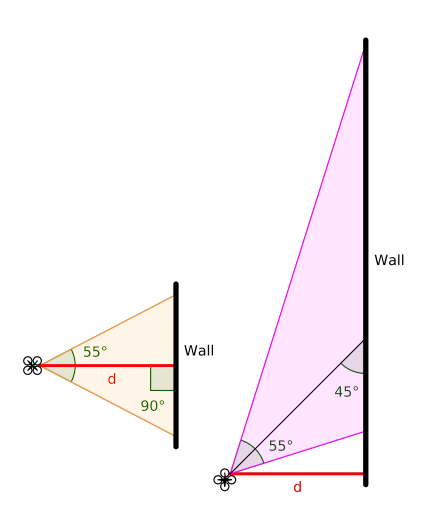


Fig. 3: The test setup, on the left, the drone is facing the wall at 90° , on the right at 45° . The distance to the wall (d) is marked in red in both scenarios.

along the slow-time reduces the noise variance significantly. We pay in a time delay for filtering along slow-time, while for filtering along fast-time, we compromise the resolution of the measured distance to the detected objects.

We chose an exponential moving average with $K_s=3$ and decided against fast time filtering $(K_f=1)$, as the additional improvements are minor compared to the costs. Compared to the baseline, the standard deviation of the motor noise is reduced by 50%, and the mean remains as unfiltered at $\sim 1700\,\mathrm{AU}$.

B. Sensor Characterization

Figure 3 shows our experimental setup for the sensor characterization. We command the drone to fly at the target height of $0.7\,\mathrm{m}$, pointing towards a wall. The sensor is positioned pointing perpendicular (90°) or in 45° towards the wall. The wall is wide enough to span the whole sensor FoV (55°). However, multipath reflections over the ground are possible and can lead to additional signal peaks.

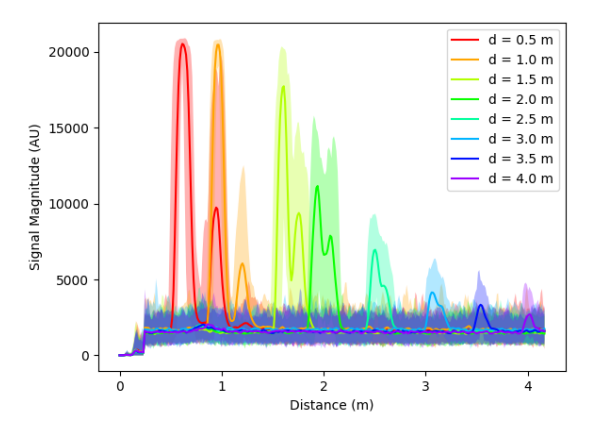


Fig. 4: Mean and min/max (shaded) for $0.5\,\mathrm{m}$ to $4\,\mathrm{m}$ distance to the wall at 90° .

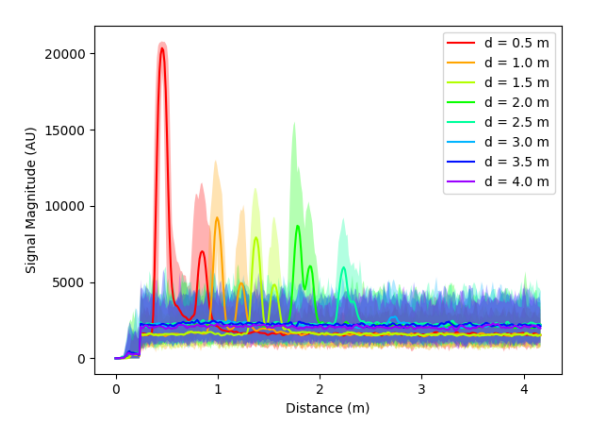


Fig. 5: Mean and min/max (shaded) for $0.5\,\mathrm{m}$ to $4\,\mathrm{m}$ distance to the wall at 45° .

During our experiments, we sweep the distance d (shown in Figure 3) between the sensor and the wall in the range $0.5\,\mathrm{m}-4\,\mathrm{m}$ with a step of $0.5\,\mathrm{m}$. For each step, we acquire 100 measurements. We use the onboard exponential moving average with $K_s=3$, shown in Section IV-A. Note that all measurements are acquired on a flying drone, leading to slight inaccuracies in position/attitude control over time. Figure 4 shows the average and min/max (shaded) of the 90° measurements. As expected, we see the noise floor at around $1700\,\mathrm{AU}$ and clear signal peaks of the wall for each distance measured.

In the 45° scenario in Figure 5, we see that the reflection causing the main peak is coming from the closest point to the sensor on the wall and not from the center of the sensor FoV. This is due to destructive interference from multiple echos along the wall superimposed on the receiving sensor.

We repeated the 90° experiment with a glass front to assess the sensor performance towards other materials. In Figure 6 the US sensor performs similarly on glass as on concrete.

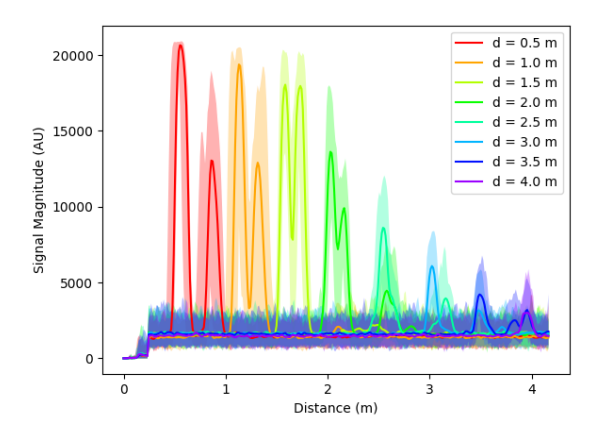


Fig. 6: Mean and min/max (shaded) for $0.55\,\mathrm{m}$ to $4\,\mathrm{m}$ distance to a glass front at 90° .

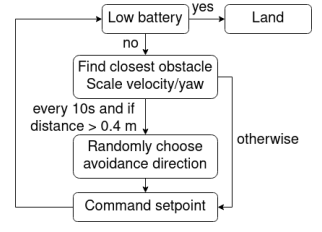


Fig. 7: Algorithmic flow of the OA implementation.

V. OA ALGORITHM IMPLEMENTATION

To evaluate the performance of the US sensor in an OA use case, we have designed and implemented an US-OA algorithm that can run directly on the ARM Cortex-M4 core on the CF, as described in Figure 7. The drone scales the velocity and yaw rate according to the distance to the closest obstacle. For random exploration, the yaw rate sign (avoiding obstacles to the left or right) is randomly chosen every $10\,\mathrm{s}$ - besides, when an obstacle is detected closer than $40\,\mathrm{cm}$, the direction is not changed to avoid turning back once the obstacle is almost avoided and staying longer than necessary close to obstacles.

The ultrasonic wave loses intensity over time, calling for lowering the threshold for object detection for longer distances. However, as every reflection but the one of the closest obstacle is irrelevant to our OA algorithm (double reflections are never the closest intensity peaks and therefore do not have to be filtered out) and we do not experience higher noise at closer distances, we decide to use a constant threshold. As shown in IV, all the (measured) noise is contained in values up to \sim 6000, so we choose $Thres_{const} = 6000$.

Once we determine the distance to the closest object, we scale the velocity in the x direction and the yaw rate accordingly. For objects detected closer than $40\,\mathrm{cm}$, we stop and only rotate with a yaw rate of $83.25\,^{\circ}\,\mathrm{s}^{-1}$ (leading to a change of $2.5\,^{\circ}$ in between measurements). We scale the yaw rate linearly for objects detected between $40\,\mathrm{cm}$ and $80\,\mathrm{cm}$ away, not turning anymore from $80\,\mathrm{cm}$ on. For

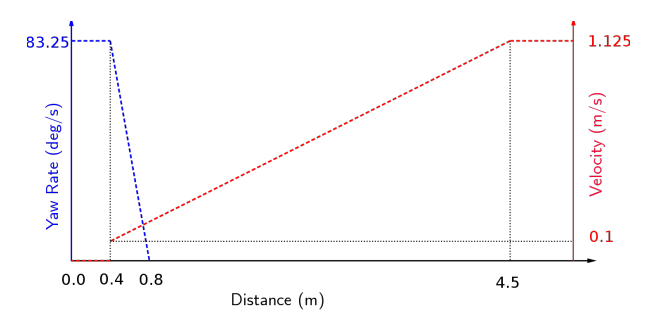


Fig. 8: Velocity and yaw rate scaling according to distance to the closest object.

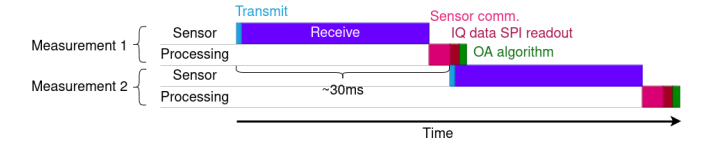


Fig. 9: Latency of transmission, reception, sensor communication, IQ data SPI readout and algorithm execution.

distances further than $40\,\mathrm{cm}$ away, we set the velocity to the distance divided by 4 per second, resulting in a maximum velocity of $1.15\,\mathrm{m/s}$. The scaling is visualized in Figure 8. To avoid sudden accelerations, we limit the velocity increase to maximally $0.05\,\mathrm{m/s}$ per measurement (equalling $1\,m/s^2$). Velocity decrements are unrestricted.

VI. EXPERIMENTAL EVALUATION

In this section, we first evaluate the power consumption, latency, memory requirements, and computational load of the ICU-30201 and the proposed OA algorithm running onboard the CF on the Cortex-M4 core. Following, we describe the in-field OA evaluation with the ICU-30201 sensor and finally compare the results to the performance of a low-power laser-based ToF sensor (VL53L1) employed for the same task, also investigating causes for failure in both sensors.

A. Power, Latency and Computational Load

For traveling twice the maximum range of 340 samples at $ODR = f_{op}/4$ in air (equalling $\sim 4.6 \,\mathrm{m}$), the ultrasonic wave needs \sim 27 ms. As we currently transmit the whole IQ data, 1.4 ms are needed for the SPI data transfer (12 MHz SPI is used). An additional $\sim 3\,\mathrm{ms}$ are used for the sensor communication before the readout (including waiting for the task to be executed by the FreeRTOS scheduler, adding a variance of \pm -- \sim 1 ms) and < 1 ms for executing the OA algorithm. However, during the SPI transfer and OA algorithm, the next measurement can already start as visualized in Figure 9, leading to a total latency of $\sim 30 \,\mathrm{ms}$ from the start of a measurement and hence a frequency of 33 Hz. As transmit and receive time are physically limited and can only be influenced by reducing the signal duration and range, only the 3 ms for the initial sensor communication could be reduced to influence the maximal measurement rate.

TABLE I: Results of 10 random exploration OA flights in an office environment.

Exp.	Time [s]	Crash	Distance [m]
(1)	430	×	107
(2)	294	√	72
(3)	392	×	120
(4)	394	×	115
(5)	188	√	55
(6)	287	×	63
(7)	35	√	8.5
(8)	97	√	27
(9)	383	×	90
(10)	115	√	27
Average	262	50%	68

As we use an exponential moving average, the OA algorithm can directly operate on the original IQ data array, and only the 20 ringdown sample magnitudes are saved until the next measurement, leading to a memory requirement of $340 \times 2 \times 2 + 20 \times 2 = 1.4 \,\mathrm{kBytes}$ for the samples in int16 format.

The OA task adds 2.5% to the STM32F405's computational load, still leaving > 57% idle. One ICU-30201 sensor consumes $<1\,\mathrm{mW}$, which is negligible on a drone using $\sim11\,\mathrm{W}$.

B. In-field OA Tests

We conducted 10 test flights in an office environment to verify our setup. The office features several desks, chairs, cupboards, glass doors, and other obstacles (a cloth rack, a bicycle, etc.). We show the results in Table I; the drone successfully flew until the battery ran low in $50\,\%$ of the tests, while it crashed in the others. The causes for the crashes were always either a soft chair or flying just below a table. The average covered distance is $68\,\mathrm{m}$, and the average flight time is 4'22''. The average time/distance until a crash (excluding battery changes) is $8'43''/136\,\mathrm{m}$.

C. Comparison to VL53L1

We repeated the real-world OA test with a VL53L1 sensor instead of the ICU-30201, operating at the same frequency (33 Hz) and using the same avoidance algorithm. Out of 10 flights, 100% were ended by a crash, traveling an average distance of $4\,\mathrm{m}$ and time of $9\,\mathrm{s}$. It is to note that the VL53L1 has not only the disadvantage of trouble with highly reflective and absorptive obstacles such as glass/black surfaces but also a more narrow FoV (27° versus 55°), which makes it almost impossible for it to perceive all obstacles it could collide with. However, most crashes were caused by glass doors.

To showcase the different perceptions of the two sensors and investigate common causes of failure, we flew along a row of different objects/materials, as displayed in Figure 10. Under the image of the scene, we show the US spectrogram and the predicted distances to the closest object from both the ICU-30201 and the VL53L1 sensors. We see the effect of the more narrow FoV of the VL53L1, enabling it to see more narrow gaps but also provoking a more risky flight behavior. While the VL53L1 fails to see the glass door and the first part of the chair, where it does not cover much of the FoV, we

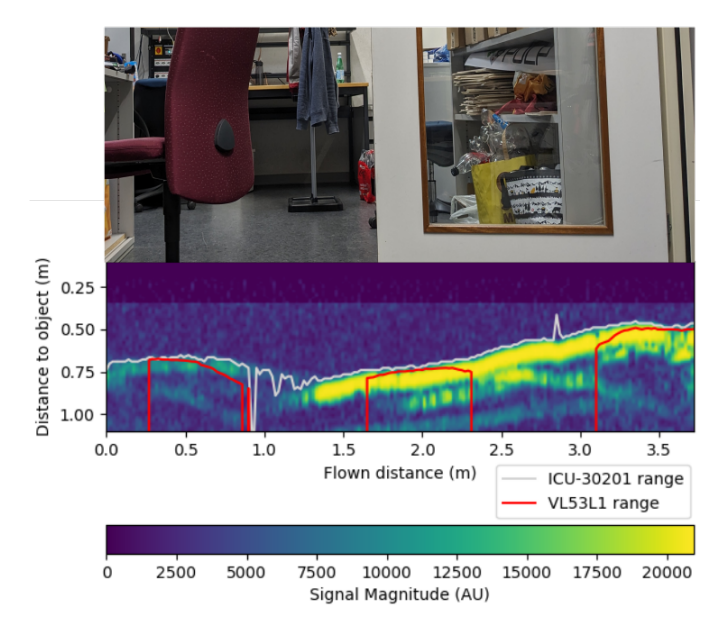


Fig. 10: ICU-30201 and VL53L1 comparison, both concurrently logged while flying at $0.1\,\rm m/s$ from the left to the right while facing the obstacles shown in the top part.

also note that while the ICU-30201 successfully detects the soft chair, it receives a much weaker reflection from it than from solid obstacles, especially when it is only at the edge of the FoV.

In terms of power consumption, the VL53L1 consumes $\sim 50 \,\mathrm{mW}$, while the ICU-30201 consumes $< 1 \,\mathrm{mW}$. However, the *BatDeck* with one sensor weighs $3 \,\mathrm{g}$, while the Multiranger deck used for the Vl53L1 experiments reduced to 1 sensor weighs only $2 \,\mathrm{g}$. Both designs can accommodate up to 4 sensors and, therefore, could be optimized for less weight.

VII. CONCLUSION

We presented and evaluated the *BatDeck*, featuring a novel, lightweight, and low-power ultrasonic sensor for expanding nano-drones. We provide a motor noise characterization and propose a filter to counteract the motor-induced vibration noise. To further characterize the sensor, we provide measurements at different distances, angles, and of different materials, proving the sensor's capabilities to detect obstacles up to 2.5 m reliably despite motor noise.

We show the OA capabilities by implementing a proof-of-concept algorithm that can run at $33\,\mathrm{Hz}$ and outperforms a classical laser-based ToF sensor, offering $50\,\%$ higher mission success rate while tracking $17\,\times$ more distance. An average flight distance of $136\,\mathrm{m}$ and time of 8'43'' until crash proves the effectiveness of US sensors for OA on nano-drones.

This work lays the foundation for the use of ultrasonic sensors on nano-drones. Future work aims to implement a self-calibration mechanism for automatic compensation of ringdown effects (improving perception of close obstacles) and motor noise. As the ICU-30201 also features a CPU, the OA algorithm could also be moved to the sensor SoC, lowering the SPI bus load and the latency.

Similarly, we aim to pursue adding multiple ultrasonic sensors, which will allow a full spatial perception of obstacles and, with this, more advanced OA algorithms. Also, using phase information and modulating the emitted US wave hold potential for improved spatial perception.

Lastly, we aim to explore sensor fusion techniques to integrate information from ultrasonic and laser-ranged ToF sensors, aiming to increase the robustness of the system when performing exploration with OA in mixed scenarios.

ACKNOWLEDGMENT

We thank TDK for their support. We also thank Christian Vogt and Christoph Leitner for their advice and help.

REFERENCES

- Statista, "Drone market size worldwide in selected years from 2021 to 2030," January 2024. [Online]. Available: https://www.statista.com/ statistics/1234521/worldwide-drone-market/
- [2] M. Hassanalian and A. Abdelkefi, "Classifications, applications, and design challenges of drones: A review," *Progress in Aerospace Sciences*, vol. 91, pp. 99–131, 2017. [Online]. Available: https://www.sciencedirect.com/science/article/pii/S0376042116301348
- [3] N. Zhang, F. Nex, G. Vosselman, and N. Kerle, "End-to-end nano-drone obstacle avoidance for indoor exploration," *Drones*, vol. 8, no. 2, 2024. [Online]. Available: https://www.mdpi.com/2504-446X/8/2/33
- [4] L. Lamberti, V. Niculescu, M. Barcis, L. Bellone, E. Natalizio, L. Benini, and D. Palossi, "Tiny-pulp-dronets: Squeezing neural networks for faster and lighter inference on multi-tasking autonomous nano-drones," in 2022 IEEE 4th International Conference on Artificial Intelligence Circuits and Systems (AICAS), 2022, pp. 287–290.
- [5] H. Müller, V. Niculescu, T. Polonelli, M. Magno, and L. Benini, "Robust and efficient depth-based obstacle avoidance for autonomous miniaturized uavs," *IEEE Transactions on Robotics*, vol. 39, no. 6, pp. 4935–4951, 2023.
- [6] K. McGuire, C. De Wagter, K. Tuyls, H. Kappen, and G. C. de Croon, "Minimal navigation solution for a swarm of tiny flying robots to explore an unknown environment," *Science Robotics*, vol. 4, no. 35, 2019.
- [7] K. Kalenberg, H. Müller, T. Polonelli, A. Schiaffino, V. Niculescu, C. Cioflan, M. Magno, and L. Benini, "Stargate: Multimodal sensor fusion for autonomous navigation on miniaturized uavs," *IEEE Internet* of Things Journal, pp. 1–1, 2024.
- [8] D. Laurijssen, R. Kerstens, G. Schouten, W. Daems, and J. Steckel, "A flexible low-cost biologically inspired sonar sensor platform for robotic applications," in 2019 International Conference on Robotics and Automation (ICRA), 2019, pp. 9617–9623.
- [9] D. Forouher, M. G. Besselmann, and E. Maehle, "Sensor fusion of depth camera and ultrasound data for obstacle detection and robot navigation," in 2016 14th International Conference on Control, Automation, Robotics and Vision (ICARCV), 2016, pp. 1–6.
- [10] V. Zhmud, N. Kondratiev, K. Kuznetsov, V. Trubin, and L. Dimitrov, "Application of ultrasonic sensor for measuring distances in robotics," in *Journal of Physics: Conference Series*, vol. 1015, no. 3. IOP Publishing, 2018, p. 032189.
- [11] M. Shen, Y. Wang, Y. Jiang, H. Ji, B. Wang, and Z. Huang, "A new positioning method based on multiple ultrasonic sensors for autonomous mobile robot," *Sensors*, vol. 20, no. 1, p. 17, 2019.
- [12] R. J. Przybyla, S. E. Shelton, C. Lee, B. E. Eovino, Q. Chau, M. H. Kline, O. I. Izyumin, and D. A. Horsley, "Mass produced micromachined ultrasonic time-of-flight sensors operating in different frequency bands," in 2023 IEEE 36th International Conference on Micro Electro Mechanical Systems (MEMS). IEEE, 2023, pp. 961–964.
- [13] D. Palossi, A. Loquercio, F. Conti, E. Flamand, D. Scaramuzza, and L. Benini, "A 64-mw dnn-based visual navigation engine for autonomous nano-drones," *IEEE Internet of Things Journal*, vol. 6, no. 5, pp. 8357– 8371, 2019.
- [14] F. Dümbgen, A. Hoffet, M. Kolundžija, A. Scholefield, and M. Vetterli, "Blind as a bat: Audible echolocation on small robots," *IEEE Robotics and Automation Letters*, vol. 8, no. 3, pp. 1271–1278, 2023.